Available online at www.sciencedirect.com

SciVerse ScienceDirect

journal homepage: www.elsevier.com/locate/he

Releasing 9.6 wt% of H_2 from $Mg(NH_2)_2$–3LiH–NH_3BH_3 through mechanochemical reaction

Hujun Cao [a,b,c], *Yongshen Chua* [b], *Yao Zhang* [d,*], *Zhitao Xiong* [b], *Guotao Wu* [b], *Jieshan Qiu* [a], *Ping Chen* [b,*]

[a] *Carbon Research Laboratory, Liaoning Key Lab for Energy Materials and Chemical Engineering, State Key Lab of Fine Chemicals, Dalian University of Technology, Dalian 116024, PR China*

[b] *Dalian National Laboratory for Clean Energy, Dalian Institute of Chemical Physics, Chinese Academy of Sciences, Dalian 116023, PR China*

[c] *University of Chinese Academy of Sciences, Beijing 100049, PR China*

[d] *School of Materials Science and Engineering, Southeast University, Nanjing 211189, PR China*

ARTICLE INFO

Article history:
Received 10 April 2013
Received in revised form
6 May 2013
Accepted 9 June 2013
Available online 12 July 2013

Keywords:
Hydrogen storage
Magnesium amide
Ammonia borane
Ball milling

ABSTRACT

Ball milling the mixture of $Mg(NH_2)_2$, LiH and NH_3BH_3 in a molar ratio of 1:3:1 results in the direct liberation of 9.6 wt% H_2 (11 equiv. H), which is superior to binary systems such as LiH–AB (6 equiv. H), AB–$Mg(NH_2)_2$ (No H_2 release) and LiH–$Mg(NH_2)_2$ (4 equiv. H), respectively. The overall dehydrogenation is a three-step process in which LiH firstly reacts with AB to yield $LiNH_2BH_3$ and $LiNH_2BH_3$ further reacts with $Mg(NH_2)_2$ to form $LiMgBN_3H_3$. $LiMgBN_3H_3$ subsequently interacts with additional 2 equivalents of LiH to form Li_3BN_2 and MgNH as well as hydrogen.

1. Introduction

The combination of $Mg(NH_2)_2$ with LiH in the molar ratio of 1:2 was recognized as a thermodynamically benign system [1,2]. It has an equilibrium hydrogen pressure over 1 bar at ca. 90 °C, which is close to the working conditions (both temperature and pressure) of proton exchange membrane (PEM) fuel cells [3]. Due to its suitable thermodynamic properties, reversibility and relatively high hydrogen content (5.6 wt%), $Mg(NH_2)_2$–2LiH is therefore regarded as a promising candidate for on-board application. However, relatively severe kinetic barrier exists in the hydrogen desorption process [4]. Over the past years, introducing catalytic and/or reactive additives appeared to be effective ways to improve the dehydrogenation/hydrogenation kinetics [5–18], however, only limited number of successful examples were observed [16,17].

NH_3BH_3 (AB in short) was intensively studied in recent years because of its extraordinarily high hydrogen capacity,

* *Corresponding authors*. Tel.: +86 411 84379905; fax: +86 411 84685940.
E-mail addresses: caohujun@gmail.com (H. Cao), zhangyao@seu.edu.cn (Y. Zhang), pchen@dicp.ac.cn (P. Chen).

0360-3199
http://dx.doi.org/10.1016/j.ijhydene.2013.06.036

i.e., 19.6 wt% [19–21]. The H bonded with N in AB molecule is positively charged ($H^{\delta+}$) while H bonded with B is negatively charged ($H^{\delta-}$) [22]. AB interacts with not only hydrides but also amides. For example, AB interacts with LiH to produce LiAB [23], AB reacts with $Mg(NH_2)_2$ to form $Mg(NH_2BH_3)_2{\cdot}2NH_3$ [24]. Considering that dehydrogenation of AB, LiAB or Mg $(NH_2BH_3)_2{\cdot}2NH_3$ is of exothermic nature [19,23,24], while $Mg(NH_2)_2$–2LiH, on the contrary, undergoes an endothermic dehydrogenation [3], a compromised thermal effect may be resulted by forming $Mg(NH_2)_2$, LiH and AB composite. In this work, we prepared the mixture of $Mg(NH_2)_2$, LiH and AB in a molar ratio of 1:3:1 through ball milling. Our results show that, instead of fine tuned thermal effect, stoichiometric interactions among $Mg(NH_2)_2$, LiH and AB leading to the release of ca. 9.6 wt% hydrogen occur during ball milling. The strong potential of forming LiAB from LiH and AB, and the subsequent reaction between LiAB and $Mg(NH_2)_2$ alter the overall reaction path of the composite.

2. Experimental

2.1. Sample preparation

$Mg(NH_2)_2$ was synthesized by reacting metallic Mg power (99%, Sigma-Adrich) with purified NH_3 (about 7 bar) at 300 °C on a self-made autoclave reactor for 7 days (Its XRD pattern was shown in Fig. #1). LiH (98%) and NH_3BH_3 (97%) were purchased from Alfa-Aesar and Sigma–Adrich, respectively. All chemicals were directly used without further treatment. The $Mg(NH_2)_2$–3LiH–AB sample was prepared by ball milling. Ball milling is one of the effective methods for conducting solid-state reactions. During ball milling, most the crystallized solid reactants become amorphous phases or liquids which facilitate reactions. On the other hand, high pressure in the order of GPa is generated in the solid by colliding balls, which can initialize the reaction [25]. The milling jar was equipped with a quick-connects (Swagelok), which can be linked to a pressure gauge (Keller) with an accuracy of 0.1 psi and enable the measurement of pressure increase in the jar caused by gas release during ball milling. The amount of hydrogen was calculated by means of the equation of state of ideal gas. Different batches of the sample were taken out from the ball milling jar after various ball milling times and were investigated by XRD, FTIR and NMR techniques. In addition, to understand the most favorable reaction pathways occurring in $Mg(NH_2)_2$–3LiH–AB sample (S1), several other samples were prepared in different methodologies, i.e., 3LiH–AB was pre-milled for 140 min, followed by adding 1 equiv. of $Mg(NH_2)_2$ (S2). Similarly, $Mg(NH_2)_2$–AB was pre-milled for 140 min and 3 equiv. of LiH was subsequently added (S3), ball milling of the equimolar of LiAB and $Mg(NH_2)_2$ (S4), the post- milled 620 min LiAB–$Mg(NH_2)_2$ ([$LiMgBN_3H_3$]) added 2 equiv. of LiH (S5) and LiAB–2LiH (S6) were prepared under the same conditions (See in Table 1).

All the samples were ball-milled at the speed of 200 rpm on a Retsch planetary ball-mill (PM400) under Ar atmosphere. The ball-to-sample weigh ratio is about 60:1. The volume of the jar is about 170 ml. To inhibit the powders conglutination and heat accumulation in the jar, the samples were milled for 1 min in one direction and halted for 15 s before it turned to reverse direction. The gaseous products generated during the ball milling were analyzed by mass spectrometer (MS), ammonia sensitive reagent (aqueous $Co(NO_3)_2$ solution) and ammonia-selective electrode. All the samples handlings were conducted in an MBRAUN glove box filled with purified argon.

2.2. Methods

The gases evolved in the ball milling were analyzed by MS (Hiden). The quantitative analysis of ammonia gas was measured on a Thermo Scientific Orion 3 Star Conductivity Benchtop Meters (USA) equipped with an NH_3-selective electrode. Diluted H_2SO_4 solution with known conductivity was used for the calibration. For the determination of NH_3 amount, the gaseous products were slowly introduced from the milling jar to 100 mL of diluted H_2SO_4 solution. The variation in conductivity due to the interaction of NH_3 and diluted H_2SO_4 solution was detected by the NH_3-selective electrode. FTIR measurements were implemented on a Varian 3100 FTIR spectrophotometer (Excalibar Series) in DRIFT mode (Diffuse Reflectance Infrared Fourier Transform). XRD measurements were conducted on a PANalytical X'pert diffractometer (Cu Kα, 40 kV, 40 mA). A self-made sample cell was used to protect the samples from air contamination during the XRD test process. Magic-angle spinning (MAS) solid-state ^{11}B and ^{7}Li NMR experiments were carried out at room temperature on a Bruker AVANCE 500 MHz NMR spectrometer (11.7 T), using a 4 mm MAS-NMR probe and ^{11}B NMR was referenced to $BF_3{\cdot}Et_2O$ at 0 ppm, ^{7}Li was referenced to 1 M aqueous solutions of lithium chloride at 0 ppm, respectively.

Table 1 – The compositions and the preparation conditions of the samples.

Samples	Initial compositions	Pre-milled time/min	The materials added after the pre-milling of the initial composition	The milling time after adding materials/min
S1	$Mg(NH_2)_2$–3LiH–NH_3BH_3	0	–	4050
S2	3LiH–NH_3BH_3	140	$Mg(NH_2)_2$	4090
S3	$Mg(NH_2)_2$–NH_3BH_3	140	3LiH	3900
S4	$LiNH_2BH_3$–$Mg(NH_2)_2$	0	–	620
S5	$LiNH_2BH_3$–$Mg(NH_2)_2$/[$LiMgBN_3H_3$]	620	2LiH	2430
S6	$LiNH_2BH_3$–2LiH	0	–	2430

3. Results and discussion

3.1. The dehydrogenation performances of $Mg(NH_2)_2$–3LiH–AB sample in the ball milling

As revealed from MS analysis (shown in Fig. 1), hydrogen was the only gaseous product released from $Mg(NH_2)_2$–3LiH–AB sample during the ball milling. Fig. 2 shows the plots of desorbed hydrogen contents as a function of ball milling time. Obviously, the interaction of the mixture $Mg(NH_2)_2$–3LiH–AB is consisted of at least two steps of dehydrogenation during the ball milling, releasing 9.6 wt% of hydrogen (10.8 equiv. H atoms) in total. This result indicates that no compromising thermal effect has taken place; instead, a different dehydrogenation pathway has occurred. Due to the high hydrogen capacity released during the ball milling, it inspires us to further investigate the reaction pathway of the system. Hydrogen was liberated rapidly at the initial stage, releasing ca. 1.1 equiv. H in the first 1 h. However, in the early stage of the second dehydrogenation step, the pressure increased gradually with increasing ball milling time. As ball milling proceeded, hydrogen released more rapidly, approaching 10.8 equiv. H. These results suggest that the interaction among $Mg(NH_2)_2$–3LiH–AB is a stepwise process and the second step encounters higher barrier than the first one. It is noteworthy that $Mg(NH_2)_2$, LiH and AB alone are stable under the same ball-milling conditions. Therefore, the hydrogen must be generated from the interactions among these reactants. According to the solid–solid reaction mechanism [4,26], the three reactants can react with one another. Based on our earlier investigations, several reactions were anticipated to occur among $Mg(NH_2)_2$, LiH and AB. LiH interacts with AB to produce LiAB (Reaction 1) [23],

$$NH_3BH_3 + LiH \rightarrow LiNH_2BH_3 + H_2 \quad (1)$$

while $Mg(NH_2BH_3)_2{\cdot}2NH_3$ can be synthesized by reacting $Mg(NH_2)_2$ with AB (Reaction 2) [24].

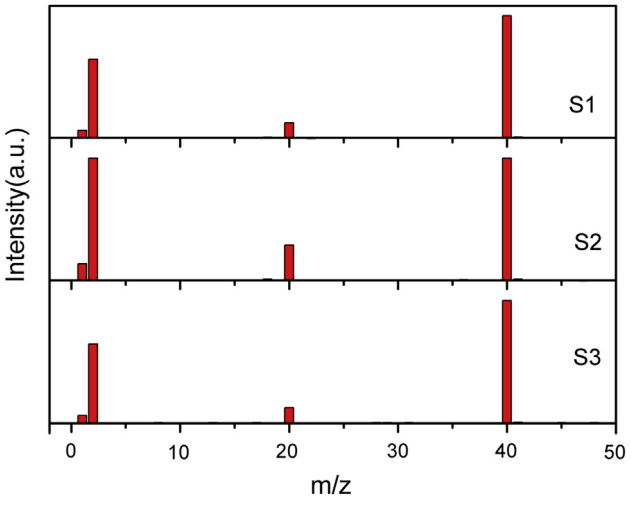

Fig. 1 – The MS signals of the samples S1, S2 and S3 after ball milling. (m/z = 1 and 2 correspond to hydrogen, m/z = 40 and 20 correspond to background, argon gas).

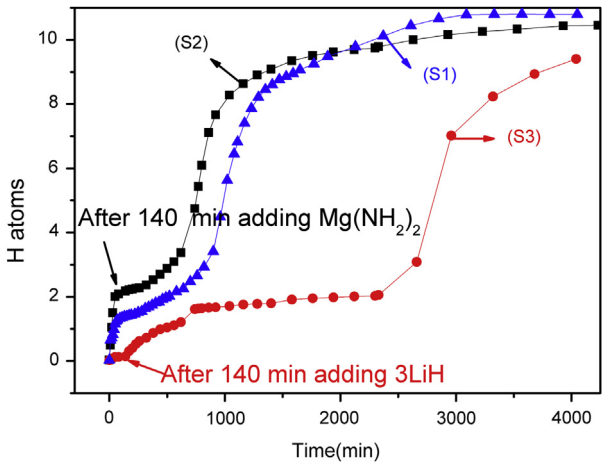

Fig. 2 – The plots of equiv. hydrogen desorbed against milling time (S1) $Mg(NH_2)_2$–3LiH–AB; (S2) 3LiH–AB was first ball milled for 140 min followed by adding equiv. $Mg(NH_2)_2$; (S3) $Mg(NH_2)_2$–AB ball milled for 140 min followed by adding 3 equiv. LiH.

$$2NH_3BH_3 + Mg(NH_2)_2 \rightarrow Mg(AB)_2{\cdot}2NH_3 \quad (2)$$

The combination of $Mg(NH_2)_2$ and LiH yields $Li_2Mg(NH)_2$ when temperature is around 180 °C. (Reaction 3) [1].

$$Mg(NH_2)_2 + 2LiH \leftrightarrow Li_2Mg(NH)_2 + 2H_2 \quad (3)$$

It is not clear how 11 equiv. H was generated under the ball milling condition. In order to clarify the mechanism for hydrogen release from the composite, we prepared the composite by two ways, 1) 3LiH–AB was initially ball milled for 140 min followed by adding equiv. $Mg(NH_2)_2$ (S2); 2) $Mg(NH_2)_2$–AB was ball milled for 140 min followed by adding 3 equiv. LiH (S3). The time dependences of hydrogen release from the samples were plotted in Fig. 2. S2 can release H 1.5 times as much as S1 (equiv. 1.4 H) in the first 1 h. However, they exhibit a similar H_2 release profiles. S3, releasing c.a. 8.1 wt% of hydrogen in total, presents a thoroughly different path from those of S1 and S2. Both hydrogen release performances and the FTIR information (shown in Fig. #2) suggest that S1 and S2 proceed in a same reaction pathway (emphasis on S2 will be shown in the next part). The firstly dehydrogenation step is mainly originated from the interaction between LiH and AB [23]. With increasing amount of LiH in the composite (LiH/AB = 3/1), the dehydrogenation proceeds faster due to the increased probability of collision between LiH and AB, thus increase the reaction rate. The second step of dehydrogenation from S1 and S2 experienced an incubation period, in which only a little hydrogen was evolved. As LiAB was formed in the first step, the second step of the dehydrogenation should come from the interaction of LiAB, $Mg(NH_2)_2$ and the excessive LiH. As shown in Fig. 2, the dehydrogenation profile of S3 differs from those of S1 and S2, in which little gas evolution was observed before the addition of LiH. Our previous study shows that when $Mg(NH_2)_2$ meets with AB, sticky matter with a composition of $Mg(NH_2BH_3)_2{\cdot}2NH_3$ will be formed [24]. After adding 3 equiv. of LiH to $Mg(NH_2BH_3)_2{\cdot}2NH_3$,

ca. 1.6 equiv. H was generated upon ca. 13 hrs of ball milling and another ca. ~8 equiv. H was evolved after ball milling for an extended period of time. Obviously, the chemical reactions that have taken place in the ball milling treatment were varied from S2 to S3. This phenomenon stimulates us to further characterize the reaction intermediates and products of S2.

Samples of S2 at different milling times were investigated by FTIR and XRD analyses. The XRD patterns show that LiAB (symbol Ψ) appears after 140-min ball milling (see Fig. 3(A)). Adding $Mg(NH_2)_2$ to the jar and milling for an additional 110 min leads to significantly weakened diffraction peaks of LiAB. At the same time, $Mg(NH_2)_2$ and LiH can be detected. After milling for a total time of 750 min, only diffraction peaks of LiH can be observed. The FTIR spectra of S2 milled for 140 min, 250 min, 750 min, 850 min and 2200 min were shown in Fig. 3(B). The sample milled for 140 min (with ca. 2.2 equiv. H released per AB-3LiH) possesses typical N–H vibrations of LiAB at 3352/3310 cm^{-1} and B–H vibrations within the range of 2000–2700 cm^{-1}. After introducing 1 equiv. of $Mg(NH_2)_2$ to the former mixture and milled for extra 110 min, the sharp vibrations of N–H bond at 3352/3310 cm^{-1} were almost undetectable. Two peaks were gradually evolved at 3327 and 3273 cm^{-1}, which are the typical N–H vibrations of $Mg(NH_2)_2$. After ball milling for 750 min, the peaks intensity of N–H and B–H vibrations decreased, implying that $Mg(NH_2)_2$ and LiAB have been consumed after their interaction. With increasing the ball milling time, an imide-like N–H vibration at around 3250 cm^{-1} was gradually developed. No B–H vibrations can be detected in the subsequent milling, indicating that LiAB were thoroughly consumed and the final product should be a B–H free species. It is noted that the vibration at 2350 cm^{-1} is likely belonged to the signal of CO_2 which come from the air. In addition, the N–H vibration at around 3250 cm^{-1} performed consistently even after prolonged ball milling, implying a stable existence of an imide species in the sample.

MAS-NMR was employed to characterize the change of ^{11}B environment in the sample against the increasing ball milling time. The post-140 min ball-milled sample which displayed a symmetric peak at −23 ppm, should belong to the boron environment of LiAB (shown in Fig. 4). It gradually disappeared with the extension of ball milling time. In contrast,

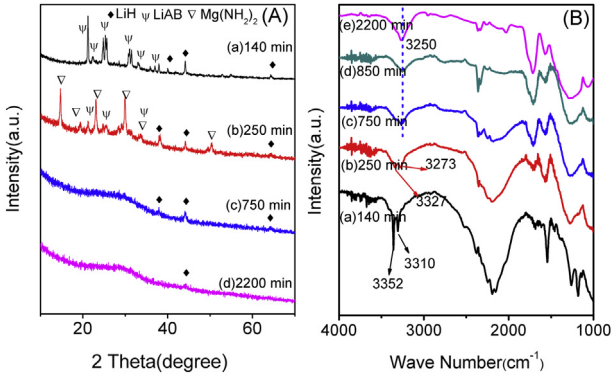

Fig. 3 – XRD patterns (A) and FTIR (B) of (S2) 3LiH–AB was first ball milled for 140 min and was followed by adding equiv. $Mg(NH_2)_2$ after ball-milled for (a) 140 min (b) 250 min (c) 750 min (d) 2200 min, respectively.

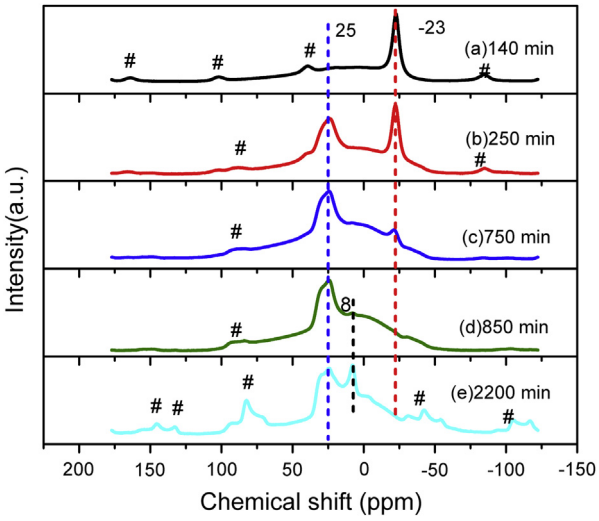

Fig. 4 – ^{11}B MAS spectra of (S2) 3LiH–AB was first ball milled for 140 min followed by adding equiv. $Mg(NH_2)_2$ after ball-milled for (a) 140 min, (b) 250 min, (c) 750 min, (d) 850 min and (e) 2200 min, respectively. # denotes the spinning sidebands.

the resonance at 25 ppm which reflects a sp^2 hybridized boron environment exists at all-time upon addition of $Mg(NH_2)_2$. This signal may be attributed to the presence of BN_3 or N_2BH species. At the end of the ball milling, only two resonances at 25 ppm and 8 ppm can be detected. By means of the results from FTIR and NMR characterizations, we deduced that a new quaternary imide was formed [$LiMgBN_3H_3$]. The resonance at ~8 ppm belongs to B–O band [27], which probably resulted from the air contamination during the samples collection.

One of the issues that should be avoided in amide-hydride system is the byproduct of ammonia, which not only damages the membrane in a fuel cell, but also leads to the cyclic instability of the material due to the loss of nitrogen [28]. In this work, NH_3-selective electrode was used to detect NH_3 concentration in the gaseous product. For S2, the NH_3 concentration in the milling jar was detected as 327.4 ppm after ball milling for 10 h. It was gradually reduced to 272.4 ppm after ball milling for 40 h. It is reasonable that large amount of amide has been converted into imide in the terminative stage of ball milling, which accounts for the substantial reduction in the NH_3 amount [29].

3.2. *The interaction between LiAB and $Mg(NH_2)_2$ in the ball milling process*

As shown above, S2 contains LiAB, $Mg(NH_2)_2$ and excess of 2 equiv. LiH before the second step dehydrogenation. Therefore, It is interesting to investigate the interactions of LiAB vs. $Mg(NH_2)_2$ and LiAB vs. LiH. The mixture of LiAB-$Mg(NH_2)_2$ was milled under the sample conditions as that of $Mg(NH_2)_2$–3LiH–AB sample. In addition, the mixture of LiAB-2LiH was also milled for comparison. Fig. 5 exhibits the time dependence of hydrogen release from LiAB-$Mg(NH_2)_2$ and LiAB-2LiH. For LiAB-$Mg(NH_2)_2$, slight pressure increase can be detected within the initial 120 min of ball milling. After

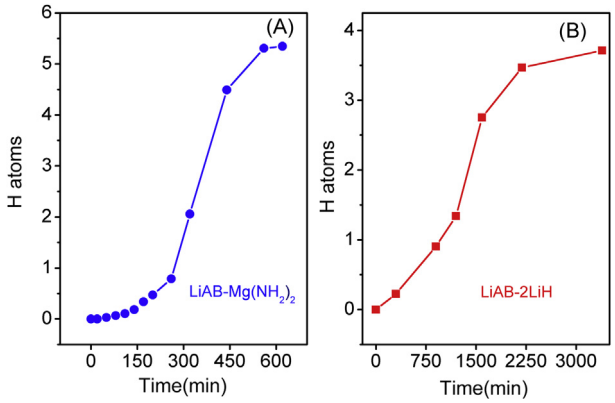

Fig. 5 – Hydrogen release with ball-milling time from (S4) LiAB-Mg(NH$_2$)$_2$ (A) and (S6) LiAB-2LiH (B).

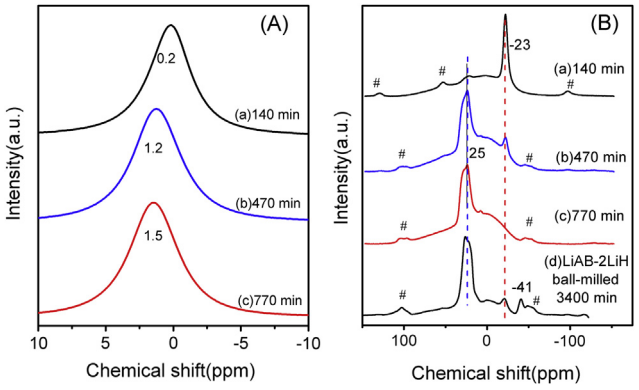

Fig. 7 – ^{7}Li MAS spectra (A) and ^{11}B MAS spectra (B) of (S4) LiAB-Mg(NH$_2$)$_2$ after ball-milled of (a) 140 min, (b) 470 min, (c) 770 min and (d) is the ^{11}B MAS spectra of (S6) LiAB-2LiH ball-milled for 3400 min # denotes the spinning sidebands.

180 min of ball-milling, hydrogen was released rapidly. After nearly 600 min of ball milling, ca. equiv. 5.5 H per LiAB-Mg(NH$_2$)$_2$ can be achieved (shown in Fig. 5(A)). Different from LiAB-Mg(NH$_2$)$_2$, the hydrogen generated from LiAB-2LiH system increased synchronously with the milling time, releasing more than 3.7 H atoms after 3400 min (shown in Fig. 5(B)).

The LiAB-Mg(NH$_2$)$_2$ samples milled at different time were collected for the XRD and FTIR analyses. Unfortunately, the samples become amorphous after milling for 470 min (shown in Fig. 6(A)). FTIR characterization revealed that the vibrations of Mg(NH$_2$)$_2$ (3273 cm^{-1}) and LiAB were (3352/3310/3295 cm^{-1}) gradually broadened during the ball milling. A broad N–H stretch centered at ca. 3250 cm^{-1} was developed, which is likely corresponded to the formation of an imide with the composition of [LiMgBN$_3$H$_3$] (shown in Fig. 6(B)). This result matches well with earlier observation in Fig. 3(B).

In order to obtain more information on the dehydrogenation process of LiAB-Mg(NH$_2$)$_2$, ^{7}Li and ^{11}B MAS-NMR measurements were employed. ^{7}Li MAS-NMR spectra (shown in Fig. 7(A)) exhibited a resonance centered at 0.2 ppm in the post-140 min milled sample. This resonance can be ascribed to the chemical shift of Li in LiAB. As milling proceeded, the ^{7}Li resonance shifted downfield, centering at 1.5 ppm at the end of ball milling. A similar ^{7}Li resonance was observed in LiMgN, implying an identical Li environment in the post milled sample. The ^{11}B MAS-NMR spectra also (Fig. 7(B)) revealed a sp^2 hybridized B environment, similar with that observed in S2 (Fig. 4). These results agree well with the earlier hypothesis on the formation of [LiMgBN$_3$H$_3$] (Reaction 4).

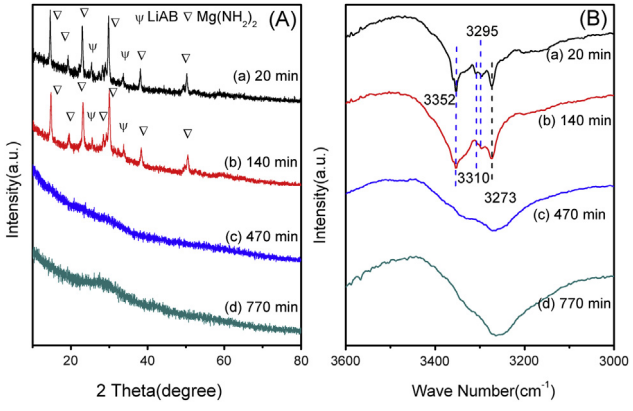

Fig. 6 – XRD patterns (A) and FTIR (B) of (S4) LiAB-Mg(NH$_2$)$_2$ after ball-milled for (a) 20 min (b) 140 min (c) 470 min (d) 770 min.

$$LiNH_2BH_3 + Mg(NH_2)_2 \rightarrow [LiMgBN_3H_3] + 3H_2 \quad (4)$$

The ^{11}B MAS spectra was also employed to characterize the post milled LiAB-2LiH sample (shown in Fig. 7(B) d). According to the detected B–N species in the spectra and the achieved amount of ca. 3.7 equiv. H in the ball milling process, it is reasonable to describe the interaction of LiAB-2LiH by Reaction 5.

$$2LiNH_2BH_3 + 2LiH \rightarrow Li_3BN_2 + LiBH_4 + 4H_2 \quad (5)$$

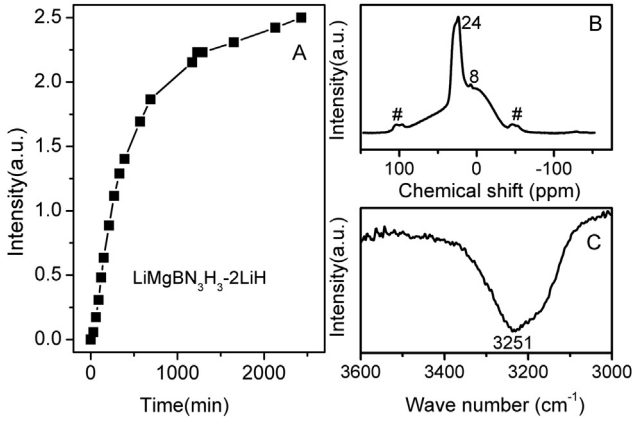

Fig. 8 – The relationship between hydrogen release amount with ball-milling time from (S5) [LiMgBN$_3$H$_3$]-2LiH (A). The ^{11}B NMR of the post-milled (S5) [LiMgBN$_3$H$_3$]-2LiH sample (B). The FTIR spectra of the post-milled (S5) [LiMgBN$_3$H$_3$]-2LiH sample (C).

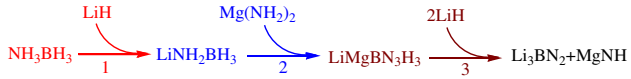

Scheme 1 – Proposed pathway of $Mg(NH_2)_2$–3LiH–NH_3BH_3 including three steps: (1) LiH reacts with NH_3BH_3 to form $LiNH_2BH_3$ and releases H_2; (2) $LiNH_2BH_3$ reacts with $Mg(NH_2)_2$ to form $LiMgBN_3H_3$ and H_2; (3) LiH reacts with $LiMgBN_3H_3$ to form Li_3BN_2, MgNH and H_2.

3.3. *The reaction of [$LiMgBN_3H_3$] and LiH in the ball milling process*

[$LiMgBN_3H_3$] yielded from ball milling LiAB-$Mg(NH_2)_2$ can further react with 2 equiv. of LiH and release additional 2.5 equiv. H when ball milling time was prolonged to 2450 min (shown in Fig. 8(A)). The finally products are composed of Li_3BN_2 and MgNH which have been characterized by ^{11}B NMR and FTIR (shown in Fig. 8(B) and (C)).

On the basis of above discussions, the interaction of [$LiMgBN_3H_3$]-2LiH can be described by Reaction 6.

$$[LiMgBN_3H_3] + 2LiH \rightarrow Li_3BN_2 + MgNH + 2H_2 \quad (6)$$

In general, the mechanochemical reaction of $Mg(NH_2)_2$–3LiH–AB can be elucidated by Reaction 7. Approximately 11 equiv. H atom (9.6 wt%) can be released during the ball milling, agreeing well with the theoretical value of 12 H atoms (pairing H^+ with H^- in the materials).

$$Mg(NH_2)_2 + 3LiH + NH_3BH_3 \rightarrow Li_3BN_2 + MgNH + 6H_2 \quad (7)$$

On the basis of above discussions, the reaction pathways are proposed and illustrated in Scheme 1.

4. Conclusions

The dehydrogenation of the composite of magnesium amide ($Mg(NH_2)_2$), lithium hydride (LiH) and ammonia borane (AB) in the molar ratio of 1:3:1 is via three steps during ball milling, i.e., LiH firstly reacts with AB to yield $LiNH_2BH_3$. The produced $LiNH_2BH_3$ further reacts with $Mg(NH_2)_2$ to form [$LiMgBN_3H_3$]. [$LiMgBN_3H_3$] subsequently interacts with 2 equiv. of LiH to form Li_3BN_2 and MgNH. This stepwise reaction results in a total release of ca. 11 equiv. H atoms (9.6 wt%) at ambient temperature.

Acknowledgments

We appreciate the financial support from the National Basic Research Program of China (Grant No. 2010CB631304), National Natural Science foundation of China (Grant Nos. 50901070, 20971120 and 21273229) and CAS-JSPS Collaborative Funding.

Appendix A. Supplementary data

Supplementary data related to this article can be found at http://dx.doi.org/10.1016/j.ijhydene.2013.06.036.

REFERENCES

[1] Xiong ZT, Wu GT, Hu JJ, Chen P. Ternary imides for hydrogen storage. Adv Mater 2004;16:1522–5.
[2] Luo WF. ($LiNH_2$–MgH_2): a viable hydrogen storage system. J Alloys Compd 2004;381:284–7.
[3] Xiong ZT, Hu JJ, Wu GT, Chen P, Luo WF, Gross K, et al. Thermodynamic and kinetic investigations of the hydrogen storage in the Li–Mg–N–H system. J Alloys Compd 2005;398:235–9.
[4] Chen P, Xiong ZT, Yang LF, Wu GT, Luo WF. Mechanistic investigations on the heterogeneous solid-state reaction of magnesium amides and lithium hydrides. J Phys Chem B 2006;110:14221–5.
[5] Liu YF, Zhong K, Luo K, Gao MX, Pan HG, Wang QD. Size-dependent kinetic enhancement in hydrogen absorption and desorption of the Li–Mg–N–H system. J Am Chem Soc 2009;131:1862–70.
[6] Hu JJ, Fichtner M, Chen P. Investigation on the properties of the mixture consisting of $Mg(NH_2)_2$, LiH, and $LiBH_4$ as a hydrogen storage material. Chem Mater 2008;20:7089–94.
[7] Shahi RR, Yadav TP, Shaz MA, Srivastva ON. Studies on dehydrogenation characteristic of $Mg(NH_2)_2$/LiH mixture admixed with vanadium and vanadium based catalysts (V, V_2O_5 and VCl_3). Int J Hydrogen Energy 2010;35:238–46.
[8] Wang JH, Hu JJ, Liu YF, Xiong ZT, Wu GT, Pan HG, et al. Effects of triphenyl phosphate on the hydrogen storage performance of the $Mg(NH_2)_2$–2LiH system. J Mater Chem 2009;19:2141–6.
[9] Hu JJ, Pohl A, Wang S, Rothe J, Fichtner M. Additive effects of $LiBH_4$ and $ZrCoH_3$ on the hydrogen sorption of the Li–Mg–N–H hydrogen storage system. J Phys Chem C 2012;116:20246–53.
[10] Ichikawa T, Tokoyoda K, Leng HY, Fujii H. Hydrogen absorption properties of Li–Mg–N–H system. J Alloys Compd 2005;400:245–8.
[11] Leng HY, Ichikawa T, Fujii H. Hydrogen storage properties of Li–Mg–N–H systems with different ratios of LiH/$Mg(NH_2)_2$. J Phys Chem B 2006;110:12964–8.
[12] Liang C, Liu YF, Wei ZJ, Jiang Y, Wu F, Gao MX, et al. Enhanced dehydrogenation/hydrogenation kinetics of the $Mg(NH_2)_2$-2LiH system with NaOH additive. Int J Hydrogen Energy 2011;36:2137–44.
[13] Aoki M, Noritake T, Nakamori Y, Towata S, Orimo S. Dehydriding and rehydriding properties of $Mg(NH_2)_2$–LiH systems. J Alloys Compd 2007;446–447:328–31.
[14] Ma LP, Dai HB, Liang Y, Kang XD, Fang ZZ, Wang PJ, et al. Catalytically enhanced hydrogen storage properties of $Mg(NH_2)_2$ + 2LiH material by graphite-supported Ru nanoparticles. J Phys Chem C 2008;112:18280–5.
[15] Price C, Gray J, Lascola Jr R, Anton DL. The effects of halide modifiers on the sorption kinetics of the Li–Mg–N–H System. Int J Hydrogen Energy 2012;37:2742–9.
[16] Wang JH, Liu T, Wu GT, Li W, Liu YF, Araújo CM, et al. Potassium-modified $Mg(NH_2)_2$/2LiH system for hydrogen storage. Angew Chem Int Ed 2009;48:5828–32.
[17] Li B, Kaye SS, Riley C, Greenberg D, Galang D, Bailey MS. Hydrogen storage materials discovery via high throughput ball milling and gas sorption. ACS Comb Sci 2012;14:352–8.
[18] Cao HJ, Zhang Y, Wang JH, Xiong ZT, Wu GT, Qiu JS, et al. Effects of Al-based additives on the hydrogen storage

performance of the $Mg(NH_2)_2$-2LiH system. Dalton Trans 2013;42(15):5524–31.
[19] Gutowska A, Li LY, Shin Y, Wang CM, Li XS, Linehan JC, et al. Nanoscaffold mediates hydrogen release and the reactivity of ammonia borane. Angew Chem Int Ed 2005;44:3578–82.
[20] Keaton RJ, Blacquiere JM, Baker RT. Base metal catalyzed dehydrogenation of ammonia-borane for chemical hydrogen storage. J Am Chem Soc 2007;129:1844–5.
[21] Marder TB. Will we soon be fueling our automobiles with ammonia-borane? Angew Chem Int Ed 2007;46(43): 8116–8.
[22] Shore SG, Parry RW. The crystalline compound ammonia-borane, 1 H_3NBH_3. J Am Chem Soc 1955;77(22):6084–5.
[23] Xiong ZT, Yong CK, Wu GT, Chen P, Shaw W, Karkamkar A, et al. High-capacity hydrogen storage in lithium and sodium amidoboranes. Nat Mater 2008;7:138–41.
[24] Chua YS, Wu GT, Xiong ZT, Karkamkar A, Guo JP, Jian MX, et al. Synthesis, structure and dehydrogenation of magnesium amidoborane monoammoniate. Chem Commun 2010;46:5752–4.
[25] Huot J, Ravnsbæk DB, Zhang J, Cuevas F, Latroche M, Jensen TR. Mechanochemical synthesis of hydrogen storage materials. Prog Mater Sci 2013;58(1):30–75.
[26] Chen P, Xiong ZT, Luo JZ, Lin JY, Tan KL. Interaction between lithium amide and lithium hydride. J Phys Chem B 2003;107:10967–70.
[27] Salentine CG. High-field ^{11}B NMR of alkali borates aqueous polyborate equilibria. Inorg Chem 1983;22:3920–4.
[28] Luo WF, Stewart K. Characterization of NH_3 formation in desorption of Li–Mg–N–H storage system. J Alloys Compd 2007;440:357–61.
[29] Hu JJ, Wu GT, Liu YF, Xiong ZT, Chen P, Wolf G. Hydrogen release from $Mg(NH_2)_2$–MgH_2 through mechanochemical reaction. J Phys Chem B 2006;110:14688–9.